Reformulation of DFT+U as a pseudo-hybrid Hubbard density functional for accelerated materials discovery

Luis A. Agapito,[1,2] Stefano Curtarolo,[2,3] and Marco Buongiorno Nardelli[4,2,*]

[1] *Department of Physics and Department of Chemistry, University of North Texas, Denton, TX 76203, USA*
[2] *Center for Materials Genomics, Duke University, Durham, NC 27708, USA*
[3] *Materials Science, Electrical Engineering, Physics and Chemistry, Duke University, Durham, NC 27708, USA*
[4] *Department of Physics, University of North Texas, Denton, TX 76203, USA*

(Dated: October 22, 2014)

The accurate prediction of the electronic properties of materials at a low computational expense is a necessary conditions for the development of effective high-throughput quantum-mechanics (HTQM) frameworks for accelerated materials discovery. HTQM infrastructures rely on the predictive capability of Density Functional Theory (DFT), the method of choice for the first principles study of materials properties. However, DFT suffers of approximations that result in a somewhat inaccurate description of the electronic band structure of semiconductors and insulators. In this article we introduce ACBN0, a pseudo-hybrid Hubbard density functional that yields an improved prediction of the band structure of insulators such as transition-metal oxides, as shown for TiO_2, MnO, NiO and ZnO, with only a *negligible* increase in computational cost.

arXiv:1406.3259v3 [cond-mat.str-el] 21 Oct 2014

INTRODUCTION

High-Throughput Quantum-Mechanics (HTQM) computation of materials properties by *ab initio* methods has become the foundation of an effective approach to materials design, discovery and characterization [1]. This data-driven approach to materials science currently presents the most promising path to the development of advanced technological materials that could solve or mitigate important social and economic challenges of the 21st century [1–11]. In order for this approach to be successful, however, one needs the confluence of three key factors: **i.** improved computational methods and tools; **ii.** greater computational power; and **iii.** heightened awareness of the power of extensive databases in science[3]. While the last two are driven by technological advances in computing and research and development needs, the development of improved computational tools appropriate for HTQM frameworks is a grand challenge that is still in need of considerable advances.

Most HTQM infrastructures rely on the predictive capability of Density Functional Theory (DFT), the method of choice for the first principles study of materials properties. However, despite the enormous success of DFT in describing many physical properties of real systems, its limitations in describing correctly the electronic band structure of insulators are well known. The method is limited by the presence of an unknown correlation term that represents the difference between the true energy of the many-body system of the electrons and the approximate energy that we can compute. The common approximations based on a nearly-homogeneous-electron-gas treatment of the electron density, the local-density (LDA) and generalized-gradient approximation (GGA), are extremely successful in the description of many physical properties of materials, but dramatically underestimate the electron energy gap in insulators and semiconductors and thus fail to satisfactorily describe the electronic properties of these systems. Higher order levels of theory that are able to predict with great accuracy the energy gaps exist (the *GW* approximation[12] and dynamical mean-field theory[13–15], among others) but they are computationally expensive and unsuitable for extensive high-throughput materials characterization [16, 17], even when Machine Learning methods are employed to simplify the complexity of the task especially when seeking for new materials systems [18, 19]. In order to address the energy gap problem at a lower computational cost the two most common corrections to traditional local and non-local approximations to DFT are "hybrid functionals" and DFT+U. Both approaches aim to reduce at some level the self-interaction error [20] and introduce the derivative discontinuity in the exchange-correlation functional[21–23] responsible for the underestimation of the energy gap[24].

Hybrid functionals are based on the idea of computing the exact exchange energy from the Kohn-Sham wavefunctions and to mix it with the (semi)local approximation of exchange energy of DFT[25]. The method is very successful in predicting the energy gap with good accuracy and points to the importance of introducing some degree of exact exchange in traditional DFT for a proper description of the electronic structure. However, the level of mixing is not determined from first principles, so the method suffers of some level of empiricism and, even after the introduction of range separated functionals suitable for periodic system calculations[26, 27], it is more computationally demanding than LDA or GGA.

The treatment of systems with strongly localized(correlated) electrons is another outstanding issue that limits the predictive power of (semi)local approximations to DFT for systems where localization is important, such as transition metal insulators, and directly impacts the

energy gap problem. The DFT+U method introduced by Liechtenstein and Anisimov [28, 29] aims at preserving the information of orbital localization from being averaged out as in LDA or GGA in order to improve the description of the band structure with a very modest increase in computational effort. Since in this paper we are mainly concerned with an extension of this approach, let us discuss its guiding principles in some detail.

Within the DFT+U ansatz, localized states φ_i largely retain their atomic nature and, therefore, can be expanded in term of an atomic-orbital basis set $\{\phi_m\} \equiv \{m\}$. The Coulomb and exchange energy associated with these states is explicitly evaluated using the Hartree-Fock (HF) framework via electron repulsion integrals (ERI, also know as two-electron integrals) with a screened (renormalized) Coulomb interaction V_{ee} and added to the original DFT energy after the removal of double counting terms in the energy expansion, in a spirit similar to the hybrid functionals approach.

The HF Coulomb and exchange energy of the localized states is given by [28]:

$$\begin{aligned} E_{\mathrm{HF}}^{\{m\}} = \frac{1}{2} \sum_{\{m\},\sigma} \{ & \langle mm'' | V_{ee} | m' m''' \rangle n^{\sigma}_{mm'} n^{-\sigma}_{m''m'''} \\ & + (\langle mm'' | V_{ee} | m' m''' \rangle - \langle mm'' | V_{ee} | m''' m' \rangle) \\ & \times n^{\sigma}_{mm'} n^{\sigma}_{m''m'''} \}, \end{aligned} \tag{1}$$

where n^{σ} is the spin density matrix n^{σ} of the atomic orbitals ϕ_m. This equation can be simplified via the introduction of the phenomenological parameters $\bar{U}$ and $\bar{J}$ that describe the on-site Hubbard-like interactions as expressed by Dudarev *et al.* [30]:

$$E_{\mathrm{HF}}^{\{m\}} \approx \frac{\bar{U}}{2} \sum_{\{m\},\sigma} N^{\sigma}_{m} N^{-\sigma}_{m'} + \frac{\bar{U} - \bar{J}}{2} \sum_{m \neq m',\sigma} N^{\sigma}_{m} N^{\sigma}_{m'}. \tag{2}$$

Here, N^{σ}_{m} is the spin occupation number of the atomic orbital ϕ_m.

From the equations above, it clearly follows that the new parameters, $\bar{U}$ and $\bar{J}$, contain the information of all the ERIs in an averaged scenario. In physical terms, $\bar{U}$ is the strong correlation experienced between localized electrons — only subtly coupled to the sea of extended states in which they live. Thus, the most akin definition of $\bar{U}$ (for the non-spin-polarized case) is the average [31]:

$$\bar{U} = \frac{1}{(2l+1)^2} \sum_{i,j} \langle \varphi_i \varphi_j | V_{ee} | \varphi_i \varphi_j \rangle, \tag{3}$$

where $2l + 1$ is the total number of localized states φ_i, and $l = 2, 3$ for d, f orbitals, respectively. The exchange contribution, $\bar{J}$, is given by a similar average [31].

Although the physical picture is clear, an unambiguous procedure for computing $\{\bar{U}, \bar{J}\}$ from *ab-initio* does not exist. Two factors need to be further clarified in Eq. 3: *i*) the screened (renormalized) Coulomb interaction V_{ee} arising from the "subtle coupling" to the background extended states; and *ii*) the actual orbitals φ_i used to represent the "localized electrons".

Amongst the most common *ab-initio* methods to compute $\bar{U}$ are the constrained random-phase approximation (cRPA) [32] and the linear-response constrained DFT (or cLDA) [33, 34]. The former computes the screened Coulomb interaction as the bare Coulomb interaction renormalized by the inverse dielectric function, which is calculated using the random phase approximation. The latter circumvents the ambiguity of V_{ee} by indirectly determining $\bar{U}$ as the second derivative of the total energy with respect to constrained variations of the atomic charge q_I of the chosen Hubbard center I, $\bar{U} = \partial^2 E / \partial {q_I}^2$. E is the total energy of a supercell large enough to converge to the bulk environment for the atom I. It is assumed that the charge perturbation on atom I does not disturb the local environment. In DFT with linear-combination-of-atomic-orbital (LCAO) basis, this is enforced by suppressing the hopping integrals to prevent charge rehybridization or transfer with its environment [33] and in the case of plane-wave DFT by subtracting a correcting term from $\partial^2 E / \partial {q_I}^2$ as given in Ref. 34. This method has been widely used for open-shell systems; nonetheless, the numerical reliability becomes challenging for closed-shell systems where the localized bands are completely full, thus exhibiting very small response to the linear perturbation [35, 36].

Regarding the representation of the φ_i states, *e.g.* d or f electrons of transition metals, localized orbitals — obtained either from the linear-muffin-tin-orbital (LMTO) method [37] or from the N^{th}-order muffin-tin-orbital (NMTO) method [38]— can be used with both the cLDA and cRPA to obtain $\bar{U}$. Recently, maximally localized Wannier functions (MLWF), an invariant choice suitable for plane-wave calculations, have also been employed [31, 39]. By construction, these functions are associated with a given angular momentum (l, m) and the direct correspondence makes them convenient to represent the localized d or f electrons. Ultimately, pinpointing a single localized state within the solid is arbitrary — any of these options are equally valid. In principle, the options should be equivalent for very localized states; nonetheless, the physical significance and construction becomes more ambiguous when bands corresponding to localized states are not fully disentangled [39]. Despite attempting the computation of the same physical entity, the cLDA and cRPA methods do not yield the same value of $\bar{U}$ [40]. Considering the number of assumptions taken in numerical implementations, the outcome is unsurprising.

In this article, we introduce an alternative *ab-initio* method to compute $\bar{U}$ and $\bar{J}$, which parallels the calculation of the HF energy for molecules and solids and follows closely the original definition of Anisimov *et al.* (Eq. 1): the Agapito-Curtarolo-Buongiorno Nardelli (ACBN0) pseudo-hybrid Hubbard density functional. In ACBN0 the Hubbard energy of DFT+U is calculated via

the direct evaluation of the local Coulomb ($\bar{U}$) and exchange ($\bar{J}$) integrals in which the screening of the bare Coulomb interaction is replaced by a renormalization of the density matrix. Through this procedure, the values of $\bar{U}$ and $\bar{J}$ are thus functionals of the electron density and depend directly on the chemical environment and crystalline field, introducing an effective procedure of giving the proper description of Mott insulators and other strongly correlated transition-metal oxides. As a first application, we discuss the electronic properties of a series of transition metal oxides that show good agreement with hybrid functionals, the *GW* approximation and experimental results at a fraction of the computational cost. In particular, we will demonstrate that the ACBN0 functional satisfies the rather ambitious criteria outlined by Pickett *et al.* in one of the first seminal articles on LDA+U [41]: *i*) ACBN0 reduces to (LDA)PBE when (LDA)PBE is known to be good; *ii*) the energy is given as a functional of the density; *iii*) the method specifies how to obtain the local orbital in question; *iv*) the definition of $\bar{U}$ and $\bar{J}$ is provided unambiguously. and *v*) the method predicts antiferromagnetic insulators when appropriate.

The article is organized as follows: the methodology is discussed in Section . The application of the method for four prototypical transition-metal oxides is presented in Section , and the results are compared against available experimental and theoretical data. Section discusses the important features of the method and suggests extensions of potential significance to the goal of discovering novel functional materials. Conclusions are summarized in Section .

METHODOLOGY

The foundations of the approach for evaluating the on-site Coulomb and exchange parameters are:

i) $\bar{U}$ and $\bar{J}$ are on-site quantities derived from the energy in the Hartree-Fock method. The HF theory considers pair-wise interactions of only two electrons at the time and therefore it misses the concept of screening. Because of this approximation, the HF theory is known to be inappropriate in describing delocalized metallic systems; however, it is qualitatively sound for molecules and insulators (especially in the strong localization regime)[42–45]. The on-site energies are derived from the HF energies following the ansatz of Mosey and Carter [46, 47] in which the occupied molecular orbitals (MO), needed for the computation of the HF energy, are considered populated only in the subspace $\{m\}$.

ii) no localized orbitals φ_i need to be explicitly computed. As in the Hartree-Fock method, all the MOs, or crystalline wavefunctions for the case of solids, are used. This eliminates the indeterminacy in finding the subset of MOs that better corresponds to the localized states, which can lead to a wide fluctuations of the calculated $\bar{U}$ [48]. During the calculation of the on-site HF energies, the localized orbitals are implicitly taken as a linear combinations the basis functions of interest, $\{m\}$, with the expansion coefficients included in the renormalized density matrix coming directly from the solution of the Kohn-Sham equations projected onto the localized basis of choice (see below);

iii) a plane-wave basis set is the natural choice for DFT calculations of periodic systems, but on-site HF energies are more efficiently computed in a localized basis set. Electron-repulsion integrals are evaluated using pseudo-atomic-orbitals (PAO) expressed as linear combination of Gaussian-type functions, that we define as the PAO-3G minimal basis set. This is possible by the projection procedure that we have recently developed [11], which seamlessly maps the plane-wave electronic structure onto a localized atomic-orbital basis set (see Appendix A). However, it is important to note that the construction of $\bar{U}$ and $\bar{J}$ outlined below is completely general and can be applied to any choice of basis, localized or otherwise.

iv) $E_{\rm HF}^{\{m\}}$ is a true functional of the electron density in the spirit of the Hohenberg-Kohn theorems. This leads to the definition of the ACBN0 pseudo-hybrid Hubbard density functional.

Calculation of the Electron Repulsion Integrals

The enormous quantity of Electron Repulsion Integrals, ERIs, needed in the calculation of the HF exchange energy is the fundamental bottleneck in the use of hybrid DFT functionals. In DFT calculations based on LCAO (PAO) basis sets, the problem is made more tractable when the PAOs are expressed as linear combinations of Gaussian-type functions, as it is commonly done in commercial packages such as Gaussian09 [49] and Crystal06 [50].

The electron repulsion integrals used in Eq. 1 are defined as four PAOs interacting under the bare Coulomb interaction $V = |\mathbf{r_1} - \mathbf{r_2}|^{-1}$ as:

$$\begin{aligned} \text{ERI} &\equiv (mm'|m''m''') \equiv \langle mm''|V|m'm'''\rangle \\ &\equiv \int d\mathbf{r_1} d\mathbf{r_2} \phi_m^*(\mathbf{r_1})\phi_{m'}(\mathbf{r_1}) V \phi_{m''}^*(\mathbf{r_2})\phi_{m'''}(\mathbf{r_2}). \quad (4) \end{aligned}$$

The real-space evaluation of these integrals is not directly possible when using a plane-wave basis set, which is the preferred choice for periodic systems. For this reason, we employ the auxiliary space of PAOs naturally included in the definition of the pseudo-potentials. Given that the radial and angular part of the PAO basis functions, $\phi_{lm}(\mathbf{r}) \equiv \frac{R_l(r)}{r} Y_l^{m\{c,s\}}(\theta,\varphi)$, are separable, they can be directly fitted using linear combinations of spherical-harmonic Gaussian functions. For efficiency, the latter functions are then further expanded as linear combination of Cartesian Gaussians defining the PAO-3G minimal basis set. (see Appendix for more technical details on these

transformations). Once expressed in the PAO-3G basis set, the ERIs can be efficiently evaluated using any optimized quantum-chemistry library. We use the C routines included in the open-source quantum-chemistry package PyQuante [51].

Hartree-Fock Coulomb and exchange energies

The knowledge of the ERIs and the molecular (or crystal) orbitals allows the calculation of the HF Coulomb and exchange energies $E_{\rm HF}$. For isolated systems (molecules or clusters) and in the restricted case:

$$\begin{aligned} E_{\rm HF}^{\rm molec.} &= \sum_{ij} N_{\psi_i} N_{\psi_j} \left[2(\psi_i\psi_i|\psi_j\psi_j) - (\psi_i\psi_j|\psi_j\psi_i)\right] \\ &= \sum_{\mu\nu\kappa\lambda} P_{\mu\nu} P_{\kappa\lambda} [2(\mu\nu|\kappa\lambda) - (\mu\lambda|\kappa\nu)]. \end{aligned} \tag{5}$$

Here $\psi_i^\sigma(\mathbf{r}) = \sum_{i,\mu} c_{\mu i}^\sigma \phi_\mu(\mathbf{r})$ are occupied molecular orbitals expanded in the PAOs' basis; $N_{\psi_i}^\sigma \equiv \sum_{i\mu\nu} c_{\mu i}^{\sigma *} S_{\mu\nu} c_{\nu i}^\sigma = 1$ is the charge of ψ_i^σ and $S_{\mu\nu}$ is the overlap integral between the PAOs ϕ_μ and ϕ_ν. The last line of Eq. 5 is expressed in the basis of atomic orbitals ϕ_μ with the density matrix $P_{\mu\nu}^\sigma = \sum_i N_{\psi_i}^\sigma c_{\mu i}^{\sigma *} c_{\nu i}^\sigma$.

The expression of the Coulomb and exchange HF energies for a periodic system is analogous to the molecular case (see Pisani *et al.* [52]):

$$E_{\rm HF}^{\rm solid} = \sum_{\substack{\mu\nu\kappa\lambda \\ \mathbf{g},\mathbf{l},\mathbf{m}}} P_{\mu\nu}^{\mathbf{g}} P_{\kappa\lambda}^{\mathbf{l}} \left[2\left(\mu^{\mathbf{0}}\nu^{\mathbf{g}}|\kappa^{\mathbf{m}}\lambda^{\mathbf{m+l}}\right) - \left(\mu^{\mathbf{0}}\kappa^{\mathbf{m}}|\nu^{\mathbf{g}}\lambda^{\mathbf{m+l}}\right)\right], \tag{6}$$

where $\mathbf{g}$, $\mathbf{m}$ and $\mathbf{l}$ are lattice vectors and $\mathbf{0}$ refers to the primitive unit cell. However, the mapping of the crystalline wavefunctions $\psi_i^{\mathbf{k}\sigma}$ in a local basis (i.e. the expansion coefficients $c_{\mu i}^{\mathbf{k}\sigma}$) is not readily available when using a plane-wave basis to solve for the electronic structure of the material as it is common for solids. We circumvent this problem by projecting the plane-wave solution into the chosen auxiliary space of PAOs following the method described in Ref. [11]. This projection procedure is a non-iterative scheme to represent the electronic ground state of a periodic system using an atomic-orbital basis, up to a predictable number of electronic states, and with controllable accuracy by filtering out high-kinetic-energy plane waves components. See Appendix for a summary of this procedure to calculate the expansion coefficients $c_{\mu i}^{\mathbf{k}\sigma}$ and the real-space density matrices of the solid, $P_{\mu\nu}^{\sigma,\mathbf{R}}$.

$\bar{U}$ and $\bar{J}$ as functional of the density: the ACBN0 functional

The energy functional for the DFT+U method is given by:

$$E_{\rm DFT+U} = E_{\rm DFT} + E_U$$

where $E_{\rm DFT}$ is the DFT energy calculated using a LDA or GGA functional. The energy correction E_U is given either in the original Anisimov-Liechtenstein [28, 29] or in the simplified Dudarev[30] formulation as:

$$E_U^{\rm Anisimov} = \left[\sum_I E_{\rm HF}^{\{m\},I}\right] - E_{\rm DC}, \tag{7a}$$

$$E_U^{\rm Dudarev} = \frac{\bar{U}-\bar{J}}{2} \sum_I \sum_{m,\sigma} \left[n_{mm}^{I\sigma} - \sum_{m'} n_{mm'}^{I\sigma} n_{m'm}^{I\sigma} \right], \tag{7b}$$

with $E_{\rm HF}^{\{m\},I}$ defined in Eq. 1 for a given atom I. $E_{\rm DC}$ corrects for a possible double counting of the localized-states interaction energy already captured (in an averaged way) in $E_{\rm DFT}$. The second formulation defines an effective on-site Coulomb interaction $U_{\rm eff} = \bar{U} - \bar{J}$ (henceforth referred simply as U). It should be noticed that numerical implementations of the Anisimov DFT+U functional (Eq. 1), for instance in QUANTUM ESPRESSO [53] or VASP [54], do not compute the ERIs explicitly. They are evaluated from tabulated Slater integrals, which ultimately depend on the provided values of $\bar{U}$ and $\bar{J}$, or from phenomenological considerations (e.g. Ref. [9 and 55]).

On the contrary, we evaluate $\bar{U}$ and $\bar{J}$ by computing directly the on-site Coulomb and exchange energies on the chosen Hubbard center, from the Coulomb and exchange Hartree-Fock energies of the solid. The following assumptions are used.

(i) We follow a central ansatz, introduced by Mosey *et al.* [46, 47] for the case of cluster calculations, that defines a "renormalized" occupation number $\overline{N}_{\psi_i}^\sigma \neq 1$ for each MO ψ_i^σ:

$$\overline{N}_{\psi_i}^\sigma \equiv \sum_{\mu\in\{\overline{m}\}} \sum_\nu c_{\mu i}^{\sigma *} S_{\mu\nu} c_{\nu i}^\sigma, \tag{8}$$

which is the Mulliken charge of the basis $\{\overline{m}\}$. The set $\{\overline{m}\}$ includes all the atomic orbitals in the unit cell that have the same quantum numbers as the orbitals $\{m\}$ of the Hubbard center of interest.

Correspondingly, we define a renormalized density matrix as:

$$\bar{P}_{\mu\nu}^\sigma \equiv \sum_i \overline{N}_{\psi_i}^\sigma c_{\mu i}^{\sigma *} c_{\nu i}^\sigma. \tag{9}$$

The renormalized occupations can be interpreted as weighting factors that specify the on-site occupation of each electronic state.

The expressions in Eqs. 8 and 9 are applicable to isolated systems (molecules and clusters). Solid-state systems are calculated in reciprocal $\mathbf{k}$-space that inherently apply periodic-boundary conditions, thus, surface effects are avoided. Periodic plane waves are the basis of choice for the solution of solid-state systems. The $\mathbf{k}$-space electronic-structure information of the material can be projected into

a PAO basis directly from the plane-wave DFT solution. We take advantage of this to compute the reduced density matrices and occupation number, needed to calculate $\bar{U}$ and $\bar{J}$, as follows

$$\bar{P}^{\sigma}_{\mu\nu} = \bar{P}^{\mathbf{0},\sigma}_{\mu\nu} = \frac{1}{\sqrt{N_{\mathbf{k}}}} \sum_{\mathbf{k},i} \overline{N}^{\mathbf{k}\sigma}_{\psi_i} c^{\mathbf{k}\sigma *}_{\mu i} c^{\mathbf{k}\sigma}_{\nu i} \tag{10a}$$

$$\overline{N}^{\mathbf{k}\sigma}_{\psi_i} = \sum_{\kappa\in\{\overline{m}\}} \sum_{\lambda} c^{\mathbf{k}\sigma *}_{\kappa i} S^{\mathbf{k}}_{\kappa\lambda} c^{\mathbf{k}\sigma}_{\lambda i} \tag{10b}$$

$$N^{\sigma}_{m} = \frac{1}{\sqrt{N_{\mathbf{k}}}} \sum_{\mathbf{k},i,\nu} c^{\mathbf{k}\sigma *}_{mi} S^{\mathbf{k}}_{m\nu} c^{\mathbf{k}\sigma}_{\nu i}. \tag{10c}$$

Here, $N_{\mathbf{k}}$ is the total number of $\mathbf{k}$-vectors in the 1^{st} Brillouin zone. See Appendix for more details.

(ii) $E^{\{m\}}_{\mathrm{HF}}$, the on-site HF energy associated to the basis $\{m\}$, is obtained from Eq. 5 by restricting the summation indexes to $\{m\}$. In the periodic case, it is reduced from Eq. 6 considering the central unit cell only, i.e. lattice vectors $\mathbf{R} = \mathbf{g} = \mathbf{l} = \mathbf{m} = \mathbf{0}$. Combining *(i)* and *(ii)*, we obtain in the general spin-unrestricted case:

$$\begin{aligned} E^{\{m\}}_{\mathrm{HF}} = \frac{1}{2} \sum_{\{m\}} & [\bar{P}^{\alpha}_{mm'} \bar{P}^{\alpha}_{m''m'''} + \bar{P}^{\alpha}_{mm'} \bar{P}^{\beta}_{m''m'''} \\ & + \bar{P}^{\beta}_{mm'} \bar{P}^{\alpha}_{m''m'''} + \bar{P}^{\beta}_{mm'} \bar{P}^{\beta}_{m''m'''}](mm'|m''m''') \\ & + \frac{1}{2} \sum_{\{m\}} [\bar{P}^{\alpha}_{mm'} \bar{P}^{\alpha}_{m''m'''} + \bar{P}^{\beta}_{mm'} \bar{P}^{\beta}_{m''m'''}](mm'''|m''m'). \end{aligned} \tag{11}$$

In this notation, each primed and unprimed index m runs over all the set $\{m\}$. Clearly, the above equation is equivalent to Anisimov's original DFT+U functional (Eq. 1) once we replace $n^{\sigma}_{mm'}$ with the renormalized density matrix $\bar{P}^{\sigma}_{mm'}$. $\sigma = \{\alpha, \beta\}$. However, while Eq. 1 requires the knowledge of a subjective screened Coulomb interaction V_{ee}, Eq. 11 uses the bare Coulomb interaction. Although screening is not considered in the HF theory, the direct parallel between both equations shows that the renormalization of the density matrix effectively introduces a degree of screening.

The comparison of Eqs. 2 with 11 leads to the definitions of $\bar{U}$ and $\bar{J}$ as density dependent quantities in the ACBN0 functional:

$$\bar{U} = \frac{\sum_{\{m\}} [\bar{P}^{\alpha}_{mm'} \bar{P}^{\alpha}_{m''m'''} + \bar{P}^{\alpha}_{mm'} \bar{P}^{\beta}_{m''m'''} + \bar{P}^{\beta}_{mm'} \bar{P}^{\alpha}_{m''m'''} + \bar{P}^{\beta}_{mm'} \bar{P}^{\beta}_{m''m'''}](mm'|m''m''')}{\sum_{m\neq m'} N^{\alpha}_{m} N^{\alpha}_{m'} + \sum_{\{m\}} N^{\alpha}_{m} N^{\beta}_{m'} + \sum_{\{m\}} N^{\beta}_{m} N^{\alpha}_{m'} + \sum_{m\neq m'} N^{\beta}_{m} N^{\beta}_{m'}}, \tag{12}$$

$$\bar{J} = \frac{\sum_{\{m\}} [\bar{P}^{\alpha}_{mm'} \bar{P}^{\alpha}_{m''m'''} + \bar{P}^{\beta}_{mm'} \bar{P}^{\beta}_{m''m'''}](mm'''|m''m')}{\sum_{m\neq m'} N^{\alpha}_{m} N^{\alpha}_{m'} + \sum_{m\neq m'} N^{\beta}_{m} N^{\beta}_{m'}}. \tag{13}$$

There are essential and relevant differences between Eqs. 12 and 13 and the similar framework of Mosey *et al.* [47]: *i*) our on-site energy requires the computation of a smaller number of electron-repulsion integrals, namely only those involving the $\{m\}$ set (i.e. 5^4 integrals for the d shell). This directly parallels the original definition of Anisimov, in sharp contrast with the methodology of Mosey *et al.* requiring ERIs between all basis functions contained in the cluster; *ii*) we consider the larger set $\{\overline{m}\}$ of localized orbitals (instead of $\{m\}$) in the calculation of the reduced occupation number given in Eq. 8; *iii*) in the Mosey *et al.* [47] approach the atom of interest is embedded in a cluster of volume large enough to yield local convergence to bulk conditions, thus requiring calculations on clusters of increasing volume to ensure convergence, which can become extremely computationally expensive; *iv*) finally, we never solve the full Hartree-Fock problem for the solid (Roothaan's equations) but project the DFT Kohn-Sham wavefunctions on the minimal PAO-3G basis set, thus implicitly including in the renormalized density matrix all the local screening effects that come from the mean field solution on the local set.

RESULTS

We selected four prototypical examples to benchmark the ACBN0 density functional: TiO_2 (rutile), MnO, NiO, and ZnO (wurtzite) are technological important transition metal oxides (TMO) that have been extensively stud-

ied both theoretically and experimentally. These materials pose a methodological challenge to traditional energy functionals (LDA or GGA) due to the strong localization of the TM-3d electrons that results in significant errors in the description of their electronic structure [56]. The set of chosen TMOs covers a wide range of 3d shell fillings, namely, $3d^2$, $3d^5$, $3d^8$, and $3d^{10}$ in Ti, Mn, Ni and Zn, respectively.

All our calculations use the Perdew-Burke-Ernzerhoff (PBE) [57] functional as a starting point and a plane wave energy cutoff of 350 Ry with a dense Monkhorst-Pack mesh to ensure good convergence of all quantities. All DFT+U calculations use the simplified rotational-invariant scheme of Dudarev [30] and Cococcioni [34] as implemented in the QUANTUM ESPRESSO package [53]. It is noticed that both the original DFT+U formulation of Anisimov and the simplified rotationally-invariant scheme are equivalent within numerical error for the same values of $\bar{U}$ and $\bar{J}$. For all elements, we used scalar-relativistic norm-conserving pseudopotential from the PSlibrary 1.0.0.[51]

Although the calculation of the effective values of $\bar{U}$ and $\bar{J}$ should be performed concurrently within the general Kohn-Sham self-consistent loop for electronic convergence, in this work we follow a simplified scheme: the initial and objective guess for the first DFT+U calculation is $U_{3d}^{(0)} = U_{2p}^{(0)} = 0$ eV. Then, the resulting electronic structure is used to compute $U^{(1)}$ for the next DFT+U step (from Eqs. 12 and 13). The process is iterated simultaneously for both transition metal and oxygen atoms until the difference between two subsequent iterations is $\left|U^{(n)} - U^{(n-1)}\right| < 10^{-4}$ eV. This self-consistent scheme ensures the internal consistency of the results while the true variational solution using the ACBN0 functional will be implemented in the near future. The converged effective values of U for the transition-metal oxides under study are reported in Table I. All the presented band structures follow the AFLOW standard integration paths [55].

In what follows, the ACBN0 results will be benchmarked against experimental measurements and higher level of theory, whenever possible. Clearly, meaningful comparisons between theory and photoemission spectra require GW quasiparticle energies (and more for excitonic effects) which go beyond DFT. Even if the DFT+U formalism has been shown to be a first-order approximation to the GW method for localized states in the static limit,[29, 58] in practice ACBN0 is clearly not nearly as inclusive and accurate as GW and a comparison between the results of the two approaches provides with a most stringent test of the validity of our method.

Titanium dioxide (rutile)

Rutile, with space group $P4_2/mnm$ (#136) is the most common form of TiO_2. We use the experimental lattice constants and internal ordering parameter of $a = b = 4.594$ Å, $c = 2.959$ Å, $\mu = 0.305$ [59]

The valence manifold is predominantly of O-2p character with small Ti-3d hybrization except at the top of the manifold at Γ, where it takes almost exclusively an O-2p character. Conversely, the unoccupied manifold is predominantly of Ti-3d character; the conduction-band minimum (CBM) is at Γ but in practice it is degenerate with the minima at R and M. Two regions are distinguishable in the 3d projected density of states (PDOS) in the unoccupied manifold (Fig. 1) and correspond to the octahedral-type crystal-field splitting of e_g (higher energy) and t_{2g} states (lower energy).

The use of an increasing on-site Coulomb potential U_{3d} on Ti alone (without correcting the oxygen) has been shown to monotonically open the gap, which reaches satisfactory accord with the experimental value of 3.03 eV [60] only at values of $U_{3d} \sim 10$ eV [61, 62]. However, Park *et al.* [63] have found that large values of the Ti on-site Coulomb interaction (> 7) introduces unphysical defect states in the study of vacancies and suggested a concomitant use of $U_{2p} = 7$ eV on oxygen is necessary to achieve both the experimental bandgap and a good treatment of vacancy states.

With small Löwdin charges of 0.29e–0.45e (out of 2e) per orbital [64], the Ti-3d states can not be considered localized and therefore the use of large values of U_{3d} is understood as an *ad hoc* fitting parameter without physical basis. Instead, each oxygen 2p orbital charge is 1.66e (out of 2e).

Our converged values for the rutile environment are Ti $U_{3d} = 0.15$ eV and O $U_{2p} = 7.34$ eV. These values yield a bandgap of 2.83 eV close to the experimental range of 2.8–3.8 eV (Table II), which improves the DFT prediction by 0.9 eV. Contrary to the predominant focus on the Ti-3d states, our results show that a correction on the oxygen 2p states can alone yield an equally satisfactory bandgap. More generally, it suggests that a correct treatment of oxygen 2p states may be more relevant to the correct modeling of TiO_2 vacancies.

The occupied O-2p PDOS [red line in Fig. 1(a)] shows a split into two regions, upper 0–3 eV and lower 3.5–6 eV, which originates in the oxygen 2p crystal-field splitting. The $2p_x$ and $2p_y$ states form sp^2-like σ bonds contained in the planar Y-shaped OTi_3 subunits whereas the $2p_z$ states remain as lone pairs perpendicular to the Y-shaped planes. The higher-energy $2p_z$ states correspond to the upper PDOS region. These nonbonding lone pairs have been explained with a simple empirical molecular-orbital model[65, 66] whereby the octahedral O_h symmetry of the local environment of each Ti coordinated to six oxygen ligands $(TiO_6)^{8-}$ frustrates the hybridization of the highest occupied orbitals[67].

Applying the on-site Coulomb potential U_{2p} on oxygen increases the localization of the $2p_z$ lone pairs, thus, increasing the splitting between the two 2p PDOS regions, cf. Figs. 1(a) and (b). The main peak of the lower PDOS

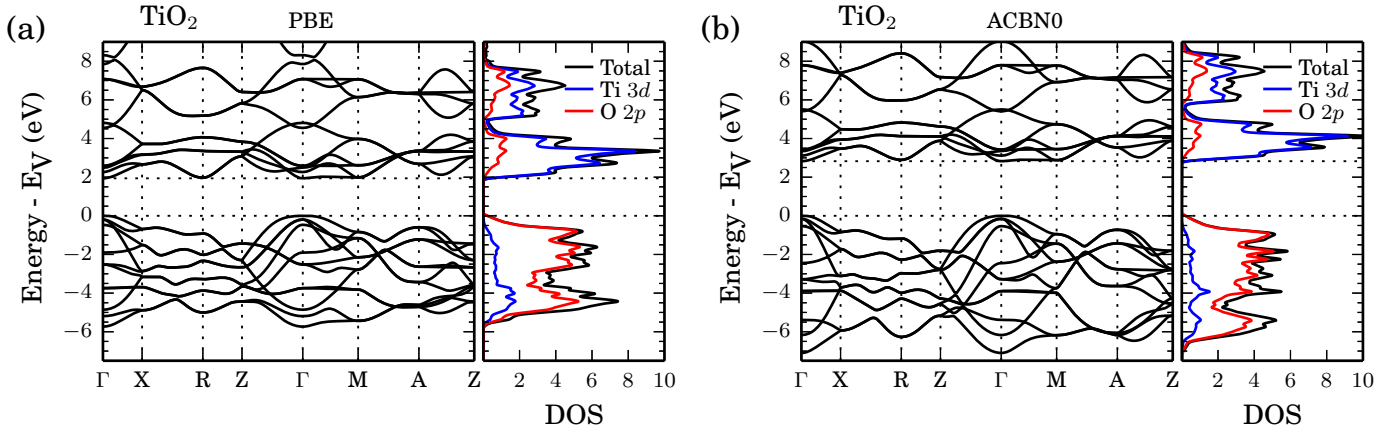

FIG. 1. Comparison between the band structures and projected density of states of TiO_2 without on-site interactions $U = 0$ (a) and with the converged effective values of $U = 0.15$ eV for Ti and 7.34 for O (b).

TABLE I. Converged values of the effective on-site Coulomb parameter U (in eV) for the transition metal (TM) $3d$ and the oxygen $2p$ states.

	TiO_2	MnO	NiO	ZnO
TM-$3d$	0.15	4.67	7.63	12.8
Oxygen $2p$	7.34	2.68	3.0	5.29

region downshifts by 1 eV, to ∼5.4 eV, consistent with the value of 5 eV reported by the accurate full-frequency-dependent *GW* calculation of Khan and Hybertsen *GW* [68] and X-ray photoelectron spectroscopy (XPS) measurements [69].

Examining the G_0W_0@GGA band structure reported by Malashevich *et al.* [70], it is interesting to notice that besides a scissor-shift operation the main correction with respect to the DFT bands is a downward energy shift of the $2p_x2p_y$ bands (lower region of the occupied manifold, -6 to -4 eV) whereas the upper region (-4 to 0 eV) remains mostly unchanged. A possible mechanism is that the *GW* approach implicitly applies a self-interaction correction that increases the splitting between the $2p_z$ and $2p_x2p_y$ states by further localizing the $2p_z$ states, which can be captured in the ACBN0 calculation.

In this regard, ACBN0 bands closely follow the G_0W_0@GGA bands of Ref. 70 in the range from -4 to 8 eV. The most significant difference happens in the remaining range of -7 to -4 eV, where our DFT+U bands are over downshifted with respect to the G_0W_0@GGA results. This can be expected from the explicit emphasis of on-site Coulomb interaction on oxygen in the ACBN0 approach.

Manganese and nickel oxides

For MnO (NiO), we use the ideal rocksalt structure with lattice constant $a = 4.4315$ Å ($a = 4.1704$ Å) [95]. The presence of type-II antiferromagnetic spin coupling along the [111] direction, below Néel temperature, effectively requires a rhombohedral primitive unit cell (RHL_1 [55], $a_{RHL} = a\sqrt{3/2}, \alpha = 33.557°$) containing 4 atoms with space group $R\bar{3}m$ (#166).

Our converged values for MnO are $U_{3d} = 4.67$ eV for Mn and $U_{2p} = 2.68$ eV for O. This value is in the range of other *ab-initio* Us reported for Mn (3.6–6.04 eV) [41, 58, 96–98]. It should be noticed that due to the different assumptions for the physical quantities (i.e. screening, localized states), *ab-initio* values of U should not be expected to the unique. A close empirical value of $U_{3d} = 4.0$ eV (albeit with no correction on oxygen) has been reported to reproduce well the experimental energy of formations of several manganese oxides [99, 100].

Both PBE and ACBN0 band structures are shown in Fig. 2. The bottom of the conduction manifold is an itinerant *sp* band with noticeable parabolic dispersion and is predominantly of Mn-4s character at CBM at Γ. The set of low-dispersion bands located above the CBM are predominantly Mn-3d t_{2g} states. These bands are more narrowly resolved in the case of NiO.

In the occupied manifold, the PBE results (gray lines) distinctly show dispersionless Mn e_g bands (separated from the rest at the top of the manifold) centered at ~ -0.5 eV and t_{2g} bands at ~ -1.5 eV. These bands have minor oxygen hybridization whereas the bands below them ($\lesssim -1.6$ eV) have a strong O-2p character. With the on-site repulsion correction in the ACBN0 results (black lines), the hybridization between Mn-3d and O-2p states increases. As a result the 3d bands are pushed down in energy while increasing their dispersion (more noticeably on the t_{2g} bands). This leads to: *i*) an increase of the bandwidth of the occupied manifold to ∼ 7.5 eV, in good agreement with results from higher levels of theory (7.6 eV *GW*@LDA+U[101] and 8 eV sX-LDA [72]), *ii*) an increase of the t_{2g} bonding-antibonding splitting across the bandgap and indirectly the resolution of the 4s parabolic

TABLE II. Minimum direct and indirect energy bandgaps (in eV).

	TiO_2	MnO		NiO		ZnO
	dir.	indir.	dir.	indir.	dir.	dir.
PBE	1.94	0.98	1.64	1.13	1.26	0.85
ACBN0	2.83	2.31	2.83	3.80	4.29	2.91
sX-LDA	3.1 [71]	2.5 [72]	3.0 [72]	4.04 [72]	4.3 [72]	3.1 [73], 3.41 [74]
HSE03	3.25 [75]	2.6 [76]	3.2 [76]	4.1 [76]	4.5 [76]	2.11 [77]
G_0W_0@GGA	3.18 [70], 3.4 [78]	1.7 [76]	2.1 [76]	1.1 [76]	1.4 [76]	2.12 [79]
G_0W_0@HSE03	3.73 [80][a]	3.4 [76]	4.0 [76]	4.7 [76]	5.2 [76]	2.97 [77]
GW@{LDA/GGA}		3.5 [81]		4.8 [81]		2.92 [82], 3.2 [79]
Exp. (XAS-XES)		4.1 [83]		4.0 [83]		3.3 [84]
Exp. (PES-BIS)	3.3±0.5 [85]	3.9 ± 0.4 [86]		4.3 [87]		
Exp. (Conductance.)		3.8–4.2 [88]		3.7 [89]		
Exp. (absorption)	3.03 [60]	3.6–3.8 [90]				3.44 [91]
Exp. (reflectance)				3.7 [92], 3.87 [93]		3.44 [94]

[a] @HSE06

band (i.e. the energy difference between the parabolic CBM at Γ and the occupied t_{2e} bands) to 2.21 eV, which compares favorably with the more rigorous self-consistent GW [81] and GW@LDA+U [101] predictions of 2.42 eV and 2.27 eV, and *iii*) an increase of the energy difference between the CBM at Γ and the unoccupied e_g bands, i.e. the bandgap.

The indirect bandgap improves from the PBE value of 0.98 eV to 2.31 eV; however, the experimental value of 3.6–4.1 eV (Table II) is still underestimated. On the other hand, the magnetic moment is evaluated to be 4.79 μ_B, which matches the experimental value (Fender *et al.* [102]).

Franchini and coauthors [100] have performed calculations with a larger value of $U_{3d} = 6.0$ eV (without U on oxygen) yielding, however, a bandgap and magnetization (2.1 eV, 4.67μ_B) smaller than our results. This evinces the importance of having the on-site Coulomb interaction not only on the TM but also on oxygen. Sakuma *et al.*[103] have shown that O 2p orbitals are considerably localized (as measured by the spread of their MLWFs) in TMOs; correspondingly, cRPA *ab-initio* calculations find the Coulomb repulsion in oxygen $\bar{U}_{2p} \gtrsim 4$ eV[97], independent of the TM. Moreover, multideterminant correlated methods (complete active space self-consistent field, CASSCF) have recently shown that, contrary to conventional wisdom, the valence-band-edge in NiO is a localized O 2p state[104].

ACBN0's MnO bandgap is closer to the predictions of hybrid functionals (sX-LDA 2.5 eV, HSE03 2.6 eV); nonetheless, the more accurate G_0W_0@HSE03 and self-consistent GW methods yield results of 3.4 and 3.5 eV, much closer to the experimental range. This underperformance of the hybrid functionals suggests that correlation effects may be particularly predominant in the case of MnO and, therefore, beyond the Hartree-exchange correction of hybrid functionals.

For NiO, PBE incorrectly locates the parabolic 4s band

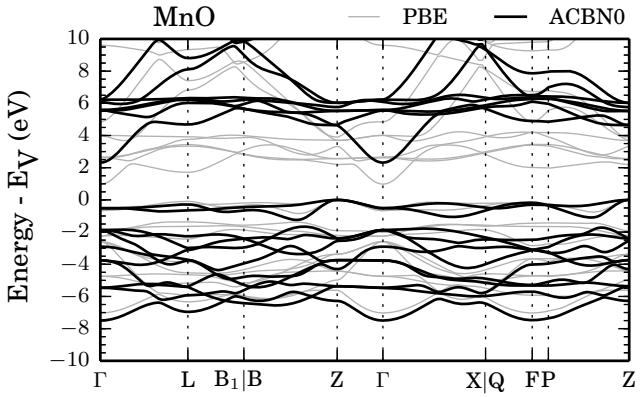

FIG. 2. Band structure (spin up) of manganese oxide. All energies are relative to the valence band maximum E_V. Effective values of $U = 4.67$ eV for the Mn-3d states and 2.68 eV for the O-2p states are used in the ACBN0 calculation.

above the 3d ones, as seen in Fig. 3. With our values of U 7.63 and 3.0 eV for Ni and O, the 4s CBM is correctly positioned at the Γ point [105], yielding an indirect bandgap (Z-Γ) of 3.8 eV and a direct gap of 4.29 eV. Considering that the 4s CBM has low spectral weight, the direct gap can well account for the dominant first peak at 4.3 eV observed with bremsstrahlung isochromat spectroscopy (BIS) [87]. Our value of Ni $U_{3d} = 7.63$ eV is in the same range than the effective value reported by Anisimov *et al.* of 7.1 eV [106], obtained with the cLDA method, widely used for *ab-initio* calculation of U. Similar to the TiO_2 case, the bands around the bottom region of the NiO occupied manifold are strongly of O-2p character and are noticeably downshifted by the use of O U_{2p} with respect to the PBE bands. The manifold bandwidth increases by 1.5 eV to 9 eV as seen in Fig. 3. Most band structures reported in the literature do not find an increase of the bandwidth; nonetheless, the same value of 9 eV is obtained with the self-consistent GW reported by Li *et al.* [105] who ar-

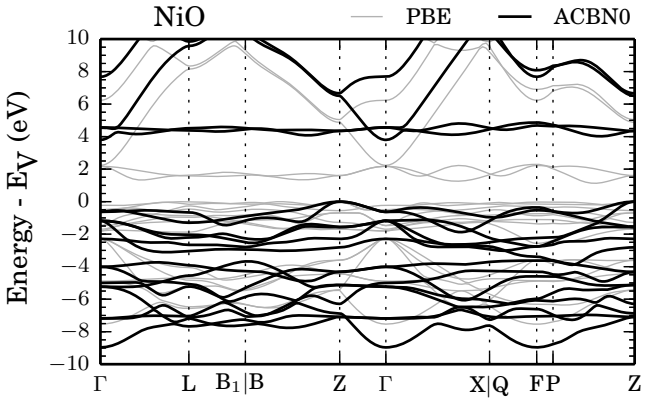

FIG. 3. Band structure (spin up) of nickel oxide. All energies are relative to the valence band maximum E_V. The effective values of $U_{3d} = 7.63$ eV for nickel and $U_{2p} = 3.0$ eV for oxygen are used in the ACBN0 calculation.

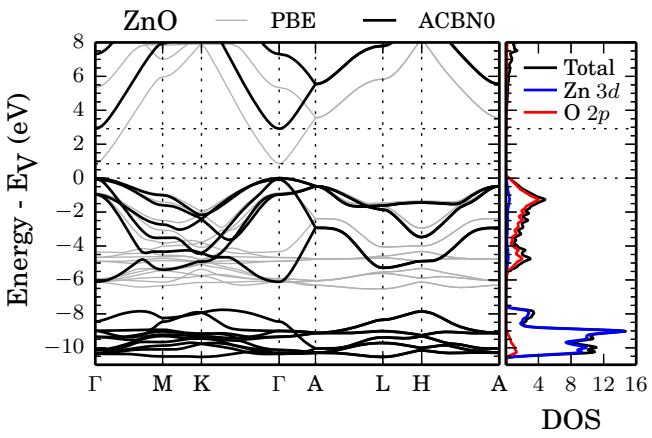

FIG. 4. Comparison between the PBE (gray) and ACBN0 (black) band structures for ZnO. The converged effective Coulomb interactions are Zn $U_{3d} = 12.8$ eV and O $U_{2p} = 5.29$ eV. The horizontal grid lines show the DFT (0.85 eV) and ACBN0 (2.91 eV) bandgaps. The panel on the right shows the projected DOS for the ACBN0 calculation

.

TABLE III. Local magnetic moments (in μ_B) for the antiferromagnetic states of MnO and NiO.

	MnO	NiO
PBE	4.58	1.49
ACBN0	4.79	1.83
HSE03	4.5 [76]	1.5 [76]
GW@LDA	4.6 [81]	1.9 [81]
Experiment	4.58 [95], 4.79 [102]	1.77 [102], 1.90 [95, 110]

gued that such broader bandwidth accounts well for the presence of strong satellite structures observed experimentally in that range of energy [87, 107]. Admittedly, these satellites are not captured in other approximations such as the model *GW* of Massidda *et al.* [108] As pointed by Gillen and Robertson [72], a bandwidth of 9 eV in NiO is in agreement with experimental measurements of 8–8.5 eV (X-ray emission spectroscopy XES [83]) and 8.5–9.5 eV (ultraviolet photoemission spectroscopy UPS [109]).

Wurtzite zinc oxide

We use a hexagonal lattice (space group #186) with relaxed lattice constants $a = b = 3.1995$ Å, $c = 5.1330$ Å, $\mu = 0.3816$, taken from the AFLOWLIB database [56] (Ref. [111], auid=aflow:b4819e0e63f994a8).

In the strongly ionic ZnO, the bands can be readily identified by their dominant orbital character. The bands in Fig. 4 (black lines) from 0 to -6 eV are mostly of O-2p character. The low-dispersion bands around -9 eV correspond to the Zn-3d states. The conduction bands are predominantly of Zn-4s character.

Within PBE, the 3d bands incorrectly overlap with the 2p manifold introducing spurious hybridizations, as shown in Fig. 4 with gray lines, which in turn leads to a strong underestimation of the bandgap. The PBE gap is 0.85 eV while the experimental gap is 3.3 eV [84]. Zinc oxide highlights the underlying failure of LDA or GGA in treating materials with localized electrons and thus constitutes a case study for the application of the DFT+U method.

Our converged values are Zn $U_{3d} = 12.8$ eV and O $U_{2p} = 5.29$ eV and yield a bandgap of 2.91 eV, which compares favorably to the experimental value. The bandwidth of the O-2p manifold shown in Fig. 4 is ~ 6 eV, in accordance to the angle-resolved photoemission spectroscopy (ARPES) value of ~ 6.05 eV [82].

Although seemingly high, our parameters agree with values reported by Calzolari *et al.* [112] ($U_{3d} = 12.0, U_{2p} = 6.5$ eV) and Ma *et al.* [113] ($U_{3d} = 10, U_{2p} = 7$ eV), both of which were found by fitting to reproduce the experimental bandgap and position of the 3d bands.

It is established that the 3d bands downshift monotonically with increasing values of U_{3d}. As the 3d bands downshift, the p–d repulsion with the O-2p bands is decreased, which in turns lowers the energy of the valence-band maximum (VBM) and, thus, monotonically increases the gap [114]. After the 3d bands have been fully disentangled from the 2p manifold, however, the 2p bands are well resolved and remain mostly insensitive to further increase of U_{3d}. Consequently, the bandgap becomes progressively independent of U_{3d} and after the 3d bands are fully disentangled the application of on-site Coulomb interaction on oxygen becomes necessary to further reach the experimental bandgap [113].

For illustration, Fig. 5 shows a comparison of the band structure with different values of U_{3d} (12.8 and 9 eV), while the U_{2d} is kept fixed at the converged value 5.29 eV. The unusual rigid shift of the U_{3d} bands seen comparing Figs. 5(a) and (b) arises from a singularity particular to

the case of the fully occupied $3d^{10}$ bands of Zn in ZnO that is rooted in the definition of the Hubbard correction to the energy functional:

$$E_U = \frac{U}{2} \sum_{I,\sigma} \sum_{m} \left[\lambda_m^{I\sigma} \left(1 - \lambda_m^{I\sigma}\right) \right],$$

which is equivalent to Eq. 7b [34], and the corresponding Hubbard potential is

$$V_U = \frac{U}{2} \sum_{I,\sigma} \sum_{m} \left(1 - 2\lambda_m^{I\sigma}\right) |\phi_m^I\rangle\langle\phi_m^I|,$$

where $0 \leq \lambda_m^{I\sigma} \leq 1$ is the occupation of the orbital ϕ_m. For fully occupied orbitals such as Zn-3d in ZnO (Löwdin charge 9.97e out of 10e), i.e. $\lambda_m \approx 1$, the Hubbard energy reduces to $E_U \approx 0$, and the Hubbard potential becomes a rigid shift $V_U \approx -U/2$ applied to the localized orbitals. In principle, at this limit, the value of U_{3d} does not change the energy of the material and becomes irrelevant in pinning the position of the 3d bands.

The experimental position of the center of the 3d bands is at -7.5 eV [82, 115] measured with respect to the VBM (E_V). Other experimental values have also been reported -8.81 eV [116], -8.6 eV [117], -7.8 eV [118]. Our value of U_{3d} underestimates the position of the 3d bands at ∼-9 eV. As discussed above, for fully disentangled and occupied 3d states, because a singularity of the DFT+U energy functional, the energy of the system becomes almost independent of U_{3d}.

Similarly, the *GW* method and hybrid functionals, while correcting the bandgap and fully disentangling the 2p and 3p manifolds, consistently miss the position of the 3d bands by ∼ 1 eV [82]. Recently, Lim *et al.* [82] proposed an assisted $GW + V_d$ approach in which the 3d bands are shifted by an *ad hoc* on-site potential $V_d = 1.5$ eV in the *GW* self-energy operator.

Analogously, the cLDA method fails in the case of Zn in ZnO. Because of the full occupancy of the 3d states, they become rather insensitive to small linear perturbations, yielding unreliable numerical values of U [36, 119]. Lee and Kim [35] have proposed an extension to cLDA method for systems with closed-shell localized electrons. They found $U_{3d} = 5.4$ eV for Zn by applying a large perturbation potential and correcting for the excess potential needed to reach the onset of the electron-density response.

DISCUSSION

Indeed, the ACBN0 functional satisfies the rather ambitious criteria outlined by Pickett *et al.*[41]:

I. *ACBN0 reduces to (LDA)PBE when (LDA)PBE is known to be good.* The reduction of $U \to 0$, arises with the introduction of the "renormalized" density-matrix $\bar{P}$ (instead of the regular density matrix P), which makes U dependent on the degree of localization of the Bloch states.

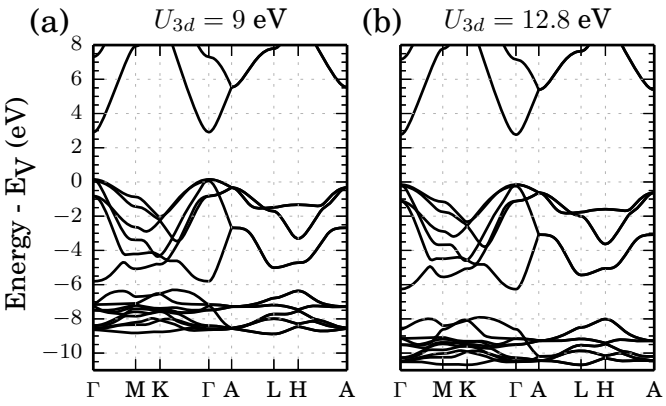

FIG. 5. Effect of the zinc on-site Coulomb repulsion U_{3d} on the occupied 3d bands. An *ad hoc* value of U_{3d}=9.0 eV (a) is compared against the converged value of 12.8 eV (b). Both cases use the converged values of U_{2d}=5.29 eV for oxygen.

A toy model with two basis functions m and m' reveals the scaling of Eq. 12 as $\bar{U} \sim \frac{1}{4} N_m N_{m'} (mm|m'm')$ in contrast to $\bar{U} \sim (mm|m'm')$ when using the regular density matrix instead. Delocalized Bloch states are assumed to be properly described at the LDA(PBE) level. The more delocalized a state, the lower the charge projected inside the atomic sphere ($N_m \approx N_{m'} \to 0$) and thereby U vanishes quadratically. See for instance the case of Ti U_{3d} in TiO_2, or silicon where ACBN0 yields $U_{2p} \approx 0$ eV.

II. *The energy is given as a functional of the density.* The value of U in ACBN0 depends only on the electron density, with a set of fixed PAOs $\{m\}$ chosen *a priori* to define U. The ACBN0 functional can be considered a zeroth-order pseudo-hybrid density functional in the sense that it includes an on-site form of the Hartree-Fock exchange. The results for the test systems studied here follow closely the more established and far computationally more expensive sX-LDA hybrid functional. Moreover, the methodology presented in this work can be immediately generalized to evaluate the nonlocal exchange energy for solids by computing the full set of required two-electron integrals. Thus, one could have a hybrid-functional plane-wave DFT calculation that is as fast as LCAO hybrid-functionals while still benefiting from the robust parallel fast-Fourier-transform algorithms and systematic basis-set convergence of plane waves.

III. *The method specifies how to obtain the local orbital in question.* ACBN0 directly parallels the original orbital-dependent DFT+U functional of Anisimov that uses atomic orbitals $\{m\}$. Conceptually, the localized states φ are linear combinations of $\{m\}$ with the expansion coefficients obtained self-consistently, thus, they reflect the chemical environment of the site; however, the expansion coefficients need not be explicitly known. Even though the information of the coefficients is conceptually included in the renormalized density matrix, they are not individually resolved. Such LCAO expansion is more general and

suitable for cases when the localized bands are not readily disentangled from other bands, which happens when the orbitals φ are not thoroughly well localized.

IV. *The definition of $\bar{U}$ and $\bar{J}$ is provided unambiguously.* See Eqs. 12 and 13.

V. *The method predicts antiferromagnetic insulators when appropriate.* This is demonstrated by the results presented for TiO_2, MnO, NiO and ZnO. The flexibility of ACBN0 is that it allows the calculation of $\bar{U}$ and $\bar{J}$ for any atom in the system of interest, yielding for instance non-negligible values for the $2p$ lone-pair of oxygen in transition metal oxides or for the p states of the anion in transition metal chalcogenides. Through the inclusion of these terms, ACBN0 corrects both the bandgap and the relative position of the different bands, in particular the ones deriving from the d orbitals of transition metal atoms. This characteristic of ACBN0 is crucial for improving the agreement with experimental results. Generally, the experimental bandgap of TMOs can not be reached if considering only the TM. Paudel and Lambrecht [120] suggested the simultaneous use of U on both the $3d$ and $4s$ orbitals of Zn to reach the experimental gap; however, a large value on Zn $U_{4s} = 43.5$ eV was needed. Finally, our results predict the stability of the antiferromagnetic phases of both MnO and NiO. However, a more thorough discussion on the relative stability of different magnetic phases will be the subject of a forthcoming publication. [121]

CONCLUSIONS

In conclusion, we have introduced ACBN0, a pseudo-hybrid density functional that incorporates the Hubbard correction of DFT+U as a natural function of the electron density and chemical environment. The values of $\bar{U}$ and $\bar{J}$ are functionals of the electron density and provide a variational way of obtaining the proper description of insulators such as transition-metal oxides. Although a more extensive validation of this functional is needed, the first results of our tests show improved agreement to higher levels of theory (hybrid functionals, the GW approximation) and to experimental measurements for the electronic properties of TMOs at a fraction of the computational cost. This is an essential requirement for the design efficient algorithms for electronic structure simulations of realistic material systems and massive high-throughput investigations [1].

We thank Drs. R. J. Mathar, N. J. Mosey, A. N. Andriotis, C. Rödl, A. Ferretti, A. Calzolari, P. Gopal, L. Liyanage, H. Shi, M. Fornari, G. Hart, O. Levy, C. Toher, D. Irving, and B. Himmetoglu for various technical discussions that have contributed to the results reported in this article. This work was supported by ONR-MURI under contract N00014-13-1-0635 and the Duke University Center for Materials Genomics. S.C. acknowledges partial support by NIST (#70NANB12H163) and DOE (DE-AC02-05CH11231, BES program under Grant #ED-CBEE). We also acknowledge the Texas Advanced Computing Center (TACC) at the University of Texas Austin for providing HPC resources, and the CRAY corporation for computational assistance.

The PAO-3G minimal basis set

The PAO basis functions $\phi_{lm}(\mathbf{r}) \equiv \frac{R_l(r)}{r} Y_l^{m\{c,s\}}(\theta,\varphi)$ are in fact obtained by solving the pseudopotential Kohn-Sham equation for a given atomic reference configuration, where $Y_l^{m\{c,s\}}$ are real-valued spherical harmonics [122]. Given that the radial and angular part are separable, they can be directly fitted using linear combinations of spherical-harmonic Gaussian functions $\mathcal{G}_s(\mathbf{r},l,m,\zeta) = r^l e^{-\zeta r^2} Y_l^{m\{c,s\}}(\theta,\varphi)$. Then, $\phi(\mathbf{r}) = \sum_{i=1}^{N_G} a_i \mathcal{G}_s(\mathbf{r},l,m,\zeta_i)$. The expansion coefficients $\{a\}$ and exponents $\{\zeta\}$ are found by fitting to $R_l(r_n)$, which is performed by using the non-linear least-square Levenberg–Marquardt algorithm to minimize the deviation

$$\sum_{r_n} \left[\sum_{i=1}^{N_G} a_i r_n^{l+1} e^{-\zeta_i r_n^2} - R_l(r_n) \right]^2 . \qquad (14)$$

$R_l(r)$ is evaluated at a logarithmic radial mesh $\{r_n\}$ and provided in the atomic pseudopotential files taken from the PSlibrary 1.0.0 [123]. We only use norm-conserving pseudopotentials since they guarantee the charge conservation of ϕ. The initial guess for the coefficients and exponents are taken from the STO-3G [124, 125] basis-set, which associates three Gaussian functions per orbital ($N_G = 3$), from the EMSL library [126].

Traditionally, Cartesian Gaussian functions of the type $\mathcal{G}_c(\mathbf{r},l_x,l_y,l_z,\zeta) = x^{l_x} y^{l_y} z^{l_z} e^{-\zeta r^2}$ are held as the most efficient basis to compute the staggering number of two-electron integrals needed in quantum chemistry calculations. We follow the procedure by Mathar [122, 127] to further convert each spherical-harmonic Gaussian into a linear combination of Cartesian Gaussians. Then, the Cartesian expansion of the PAOs is

$$\phi_{lm}(\mathbf{r}) = \frac{1}{4}\sqrt{\frac{(2l+1)!!}{\pi N_{l,m}}} f_{l,m}(x,y,z) \sum_{i=1}^{N_G} a_i e^{-\zeta_i r^2}, \qquad (15)$$

where $f_{l,m}(x,y,z)$ is given in Table IV.

An example of this fitting procedure is shown in Figure 6 for Zn-$3d$ and O-$2p$ PAO. Having the PAOs expressed as linear combination of Gaussian-type orbitals in Eq. 15 is largely advantageous, since it allows computation of the ERIs in a straightforward and analytical way. Furthermore Gaussians allow filtering out ERIs with negligible energy contribution [128] further speeding up calculations, as implemented in the Heyd-Scuseria-Ernzerhof HSE03 [26] hybrid functional.

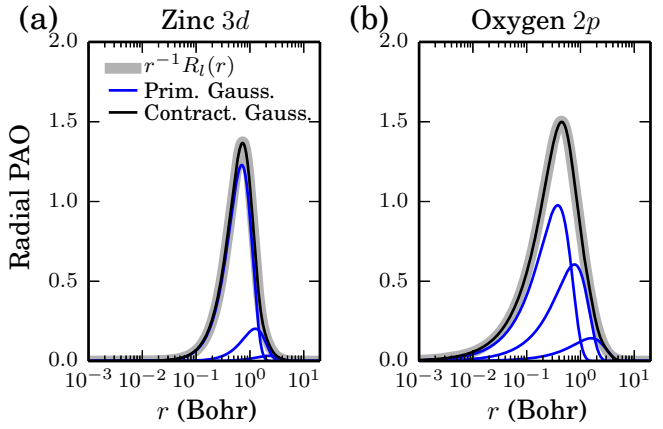

FIG. 6. Fitting the radial component of the PAOs ($r^{-1}R_l(r)$, yellow line) as a linear combination of primitive Gaussians (black line). Each contracted Gaussian is the sum of the three primitive Gaussians shown in blue. The Zn d (a) and O p PAOs (b) are taken from the PSlibrary 1.0.0.

TABLE IV. Cartesian expansion of $f_{l,m}$

(l,m)	$N_{l,m}$	$f_{l,m}(x,y,z)$
(0, 0)	0.25	1
(1,-1)	0.25	y
(1, 0)	0.25	z
(1, 1)	0.25	x
(2,-2)	0.25	xy
(2,-1)	0.25	yz
(2, 0)	3	$2z^2-x^2-y^2$
(2, 1)	0.25	xz
(2, 2)	1	x^2-y^2

Calculation of the real-space Hamiltonian and density matrices from the plane-wave electronic structure

The solid is efficiently calculated using plane-wave DFT on a unit cell with periodic boundary conditions. The plane-wave basis allows a systematic convergence of the basis-set energy error, which is controlled by a single energy-cutoff parameter. Periodic-boundary conditions are implicit to the plane-wave basis, thus avoiding the presence of surface effects intrinsic to molecular cluster calculations. Moreover, plane waves allow the use robust and scalable Fourier-transform algorithms. We follow the method described in Ref. [11] to project the **k**-space electronic structure of the solid onto an atomic-orbital space by filtering out high-kinetic-energy plane waves. The resulting reciprocal-space Hamiltonian $H^{\sigma,\mathbf{k}}$ and overlap $S^{\mathbf{k}}$ matrices are then Fourier-transformed into real space resulting in:

$$H^{\sigma,\mathbf{0R}} = \frac{1}{\sqrt{N_{\mathbf{k}}}} \sum_{\mathbf{k}} e^{-i\mathbf{k}\cdot\mathbf{R}} S^{\mathbf{k}\,\frac{1}{2}} H^{\sigma,\mathbf{k}}(\kappa, N) S^{\mathbf{k}\,\frac{1}{2}}, \qquad (16)$$

$$S^{\mathbf{0R}} = \frac{1}{\sqrt{N_{\mathbf{k}}}} \sum_{\mathbf{k}} e^{-i\mathbf{k}\cdot\mathbf{R}} S^{\mathbf{k}}. \qquad (17)$$

The parameters κ and N, defined in Ref. 11, determine the shifting and filtering for the projection procedure. The overlap integral between a basis function ϕ_μ located inside the primitive unit cell (lattice vector **0**) and the periodic translation of ϕ_ν to lattice vector **R** is the matrix element $S^{\mathbf{0R}}_{\mu\nu} = \langle \mu^{\mathbf{0}} | \nu^{\mathbf{R}} \rangle$.

The real-space density matrix is then computed as:

$$P^{\sigma,\mathbf{0R}}_{\mu\nu} = \frac{1}{\sqrt{N_{\mathbf{k}}}} \sum_{\mathbf{k},i} e^{-i\mathbf{k}\cdot\mathbf{R}} N^{\mathbf{k}\sigma}_{\psi_i} c^{\mathbf{k}\sigma}_{\mu i} c^{\mathbf{k}\sigma}_{\nu i}, \qquad (18)$$

where $N^{\mathbf{k}\sigma}_{\psi_i} = 1$ for all occupied states $\psi^{\mathbf{k}\sigma}_i$. The expansion coefficients $c^{\mathbf{k}\sigma}_{\mu i}$ are the components of the generalized eigenvectors of $H^{\sigma,\mathbf{k}}$ and $S^{\mathbf{k}}$.

* mbn@unt.edu

[1] S. Curtarolo, G. L. W. Hart, M. Buongiorno Nardelli, N. Mingo, S. Sanvito, and O. Levy, *The high-throughput highway to computational materials design*, Nat. Mater. **12**, 191–201 (2013).

[2] Office of Science and Technology Policy, White House, *Materials Genome Initiative for Global Competitiveness*, http://www.whitehouse.gov/mgi (2011).

[3] Editorial, *Fuelling discovery by sharing*, Nat. Mater. **12**, 173 (2013).

[4] G. Ceder and K. Persson, *How Supercomputers Will Yield a Golden Age of Materials Science*, Scientific American (Dec 2013).

[5] J. Greeley, T. F. Jaramillo, J. Bonde, I. Chorkendorff, and J. K. Nørskov, *Computational high-throughput screening of electrocatalytic materials for hydrogen evolution*, Nat. Mater. **5**, 909–913 (2006).

[6] K. Yang, W. Setyawan, S. Wang, M. Buongiorno Nardelli, and S. Curtarolo, *A search model for topological insulators with high-throughput robustness descriptors*, Nat. Mater. **11**, 614–619 (2012).

[7] R. Armiento, B. Kozinsky, M. Fornari, and G. Ceder, *Screening for high-performance piezoelectrics using high-throughput density functional theory*, Phys. Rev. B **84**, 014103 (2011).

[8] W. Setyawan, R. M. Gaume, S. Lam, R. S. Feigelson, and S. Curtarolo, *High-Throughput Combinatorial Database of Electronic Band Structures for Inorganic Scintillator Materials*, ACS Comb. Sci. **13**, 382–390 (2011).

[9] S. Wang, Z. Wang, W. Setyawan, N. Mingo, and S. Curtarolo, *Assessing the thermoelectric properties of sintered compounds via high-throughput ab-initio calculations*, Phys. Rev. X **1**, 021012 (2011).

[10] L. Yu and A. Zunger, *Identification of Potential Photovoltaic Absorbers Based on First-Principles Spectroscopic Screening of Materials*, Phys. Rev. Lett. **108**, 068701 (2012).

[11] L. A. Agapito, A. Ferretti, A. Calzolari, S. Curtarolo, and M. Buongiorno Nardelli, *Effective and accurate represen-*

tation of extended Bloch states on finite Hilbert spaces, Phys. Rev. B **88**, 165127 (2013).

[12] L. Hedin, *New Method for Calculating the One-Particle Green's Function with Application to the Electron-Gas Problem*, Phys. Rev. **139**, A796–A823 (1965).

[13] A. Georges and G. Kotliar, *Hubbard model in infinite dimensions*, Phys. Rev. B **45**, 6479–6483 (1992).

[14] A. Georges, G. Kotliar, W. Krauth, and M. J. Rozenberg, *Dynamical mean-field theory of strongly correlated fermion systems and the limit of infinite dimensions*, Rev. Mod. Phys. **68**, 13–125 (1996).

[15] G. Kotliar, S. Y. Savrasov, K. Haule, V. S. Oudovenko, O. Parcollet, and C. A. Marianetti, *Electronic structure calculations with dynamical mean-field theory*, Rev. Mod. Phys. **78**, 865–951 (2006).

[16] G. L. W. Hart, S. Curtarolo, T. B. Massalski, and O. Levy, *Comprehensive Search for New Phases and Compounds in Binary Alloy Systems Based on Platinum-Group Metals, Using a Computational First-Principles Approach*, Phys. Rev. X **3**, 041035 (2013).

[17] C. Toher, J. J. Plata, O. Levy, M. de Jong, M. D. Asta, M. Buongiorno Nardelli, and S. Curtarolo, *High-Throughput Computational Screening of thermal conductivity, Debye temperature and Grüneisen parameter using a quasi-harmonic Debye Model*, in press, Phys. Rev. B p. arxiv.org/abs/1407.7789 (2014).

[18] J. Carrete, W. Li, N. Mingo, S. Wang, and S. Curtarolo, *Finding unprecedentedly low-thermal-conductivity half-Heusler semiconductors via high-throughput materials modeling*, Phys. Rev. X **4**, 011019 (2014).

[19] J. Carrete, N. Mingo, S. Wang, and S. Curtarolo, *Nanograined Half-Heusler Semiconductors as Advanced Thermoelectrics: An Ab Initio High-Throughput Statistical Study*, Adv. Funct. Mater. p. 10.1002/adfm.201401201 (2014).

[20] J. P. Perdew and A. Zunger, *Self-interaction correction to density-functional approximations for many-electron systems*, Phys. Rev. B **23**, 5048 (1981).

[21] J. P. Perdew and M. Levy, *Physical content of the exact Kohn-Sham orbital energies: band gaps and derivatives discontinuities*, Phys. Rev. Lett. **51**, 1884 (1983).

[22] L. J. Sham and M. Schluter, *Density functional theory of the energy gap*, Phys. Rev. Lett. **51**, 1888 (1983).

[23] J. P. Perdew, R. B. Parr, M. Levy, and J. L. Balduz, *Density-Functional Theory for Fractional Particle Number: Derivative Discontinuities of the Energy*, Phys. Rev. Lett. **49**, 1691–1694 (1982).

[24] V. Ivády, R. Armiento, K. Szász, E. Janzén, A. Gali, and I. A. Abrikosov, *Theoretical unification of hybrid-DFT and DFT+U methods for the treatment of localized orbitals*, Phys. Rev. B **90**, 035146 (2014).

[25] S. Kümmel and L. Kronik, *Orbital-dependent density functionals: Theory and applications*, Rev. Mod. Phys. **80**, 3–60 (2008).

[26] J. Heyd, G. E. Scuseria, and M. Ernzerhof, *Hybrid functionals based on a screened Coulomb potential*, J. Chem. Phys. **118**, 8207–8215 (2003).

[27] J. Heyd, G. E. Scuseria, and M. Ernzerhof, *Erratum: "Hybrid functionals based on a screened Coulomb potential" [J. Chem. Phys.118, 8207 (2003)]*, J. Chem. Phys. **124**, 219906 (2006).

[28] A. I. Liechtenstein, V. I. Anisimov, and J. Zaanen, *Density-functional theory and strong interactions: Orbital ordering in Mott-Hubbard insulators*, Phys. Rev. B **52**, R5467–R5470 (1995).

[29] V. I. Anisimov, F. Aryasetiawan, and A. I. Lichtenstein, *First-principles calculations of the electronic structure and spectra of strongly correlated systems: the LDA + U method*, J. Phys.: Cond. Mat. **9**, 767 (1997).

[30] S. L. Dudarev, G. A. Botton, S. Y. Savrasov, C. J. Humphreys, and A. P. Sutton, *Electron-energy-loss spectra and the structural stability of Nickel oxide: An LSDA+U study*, Phys. Rev. B **57**, 1505–1509 (1998).

[31] B.-C. Shih, Y. Zhang, W. Zhang, and P. Zhang, *Screened Coulomb interaction of localized electrons in solids from first principles*, Phys. Rev. B **85**, 045132 (2012).

[32] M. Springer and F. Aryasetiawan, *Frequency-dependent screened interaction in Ni within the random-phase approximation*, Phys. Rev. B **57**, 4364–4368 (1998).

[33] O. Gunnarsson, O. K. Andersen, O. Jepsen, and J. Zaanen, *Density-functional calculation of the parameters in the Anderson model: Application to Mn in CdTe*, Phys. Rev. B **39**, 1708–1722 (1989).

[34] M. Cococcioni and S. de Gironcoli, *Linear response approach to the calculation of the effective interaction parameters in the* LDA+U *method*, Phys. Rev. B **71**, 035105 (2005).

[35] W.-J. Lee and Y.-S. Kim, *Linear-response calculation of the effective coulomb interaction between closed-shell localized electrons: Cu, Zn, and ZnO*, Journal of the Korean Physical Society **60**, 781–786 (2012).

[36] B. Himmetoglu, A. Floris, S. de Gironcoli, and M. Cococcioni, *Hubbard-corrected DFT energy functionals: The LDA+U description of correlated systems*, International Journal of Quantum Chemistry **114**, 14–49 (2014).

[37] F. Aryasetiawan and O. Gunnarsson, *Linear-muffin-tin-orbital method with multiple orbitals per L channel*, Phys. Rev. B **49**, 7219–7232 (1994).

[38] O. K. Andersen and T. Saha-Dasgupta, *Muffin-tin orbitals of arbitrary order*, Phys. Rev. B **62**, R16219–R16222 (2000).

[39] T. Miyake, F. Aryasetiawan, and M. Imada, *Ab initio procedure for constructing effective models of correlated materials with entangled band structure*, Phys. Rev. B **80**, 155134 (2009).

[40] F. Aryasetiawan, K. Karlsson, O. Jepsen, and U. Schönberger, *Calculations of Hubbard U from first-principles*, Phys. Rev. B **74**, 125106 (2006).

[41] W. E. Pickett, S. C. Erwin, and E. C. Ethridge, *Reformulation of the LDA+U method for a local-orbital basis*, Phys. Rev. B **58**, 1201 (1998).

[42] R. Orlando, R. Dovesi, C. Roetti, and V. R. Saunders, *Ab initio Hartree-Fock calculations for periodic compounds: application to semiconductors*, J. Phys.: Conden. Matt. **2**, 7769 (1990).

[43] R. Dovesi, C. Roetti, E. A. C. Freyria-Fava, and V. R. S. N. M. Harrison, *Ab initio Hartree-Fock treatment of ionic and semi-ionic compounds: state of the art*, Phil. Trans. R. Soc. A **341**, 203–210 (1992).

[44] R. Dovesi, M. Causa, R. Orlando, C. Roetti, and V. R. Saunders, *Ab initio approach to molecular crystals: A periodic Hartree-Fock study of crystalline urea*, J. Chem. Phys. **92**, 7402–7411 (1990).

[45] R. Dovesi, R. Orlando, C. Roetti, C. Pisani, and V. R. Saunders, *The periodic Hartree-Fock method and its implementation in the Crystal code*, Phys. Stat. Solidi B **217**, 63–88 (2000).

[46] N. J. Mosey and E. A. Carter, *Ab initio evaluation of*

Coulomb and exchange parameters for DFT+U calculations, Phys. Rev. B **76**, 155123 (2007).

[47] N. J. Mosey, P. Liao, and E. A. Carter, *Rotationally invariant ab initio evaluation of Coulomb and exchange parameters for DFT+U calculations*, J. Chem. Phys. **129**, 014103 (2008).

[48] A. N. Andriotis, R. M. Sheetz, and M. Menon, *LSDA+U method: A calculation of the U values at the Hartree-Fock level of approximation*, Phys. Rev. B **81**, 245103 (2010).

[49] M. J. Frisch, G. W. Trucks, H. B. Schlegel, G. E. Scuseria, M. A. Robb, J. R. Cheeseman, G. Scalmani, V. Barone, B. Mennucci, G. A. Petersson, H. Nakatsuji, M. Caricato, X. Li, H. P. Hratchian, A. F. Izmaylov, J. Bloino, G. Zheng, J. L. Sonnenberg, M. Hada, M. Ehara, K. Toyota, R. Fukuda, J. Hasegawa, M. Ishida, T. Nakajima, Y. Honda, O. Kitao, H. Nakai, T. Vreven, J. A. Montgomery Jr., J. E. Peralta, F. Ogliaro, M. Bearpark, J. J. Heyd, E. Brothers, K. N. Kudin, V. N. Staroverov, R. Kobayashi, J. Normand, K. Raghavachari, A. Rendell, J. C. Burant, S. S. Iyengar, J. Tomasi, M. Cossi, N. Rega, J. M. Millam, M. Klene, J. E. Knox, J. B. Cross, V. Bakken, C. Adamo, J. Jaramillo, R. Gomperts, R. E. Stratmann, O. Yazyev, A. J. Austin, R. Cammi, C. Pomelli, J. W. Ochterski, R. L. Martin, K. Morokuma, V. G. Zakrzewski, G. A. Voth, P. Salvador, J. J. Dannenberg, S. Dapprich, A. D. Daniels, O. Farkas, J. B. Foresman, J. V. Ortiz, J. Cioslowski, and D. J. Fox, *Gaussian09 Revision D.01*. Gaussian Inc. Wallingford CT 2009.

[50] R. Dovesi, V. R. Saunders, C. Roetti, R. Orlando, C. M. Zicovich-Wilson, F. Pascale, B. Civalleri, K. Doll, N. M. Harrison, I. J. Bush, P. D'Arco, and M. Llunell, *CRYSTAL06 User's Manual (University of Torino, Torino, 2006)*.

[51] Richard P. Muller, PyQuante 1.6.4: Python Quantum Chemistry `http://pyquante.sourceforge.net/`.

[52] C. Pisani and R. Dovesi, *Exact-exchange Hartree-Fock calculations for periodic systems. I. Illustration of the method*, Int. J. Quantum. Chem. **17**, 501–516 (1980).

[53] P. Giannozzi, S. Baroni, N. Bonini, M. Calandra, R. Car, C. Cavazzoni, D. Ceresoli, G. L. Chiarotti, M. Cococcioni, I. Dabo, A. Dal Corso, S. de Gironcoli, S. Fabris, G. Fratesi, R. Gebauer, U. Gerstmann, C. Gougoussis, A. Kokalj, M. Lazzeri, L. Martin-Samos, N. Marzari, F. Mauri, R. Mazzarello, S. Paolini, A. Pasquarello, L. Paulatto, C. Sbraccia, S. Scandolo, G. Sclauzero, A. P. Seitsonen, A. Smogunov, P. Umari, and R. M. Wentzcovitch, *QUANTUM ESPRESSO: a modular and open-source software project for quantum simulations of materials*, J. Phys.: Conden. Matt. **21**, 395502 (2009).

[54] G. Kresse and J. Furthmüller, *Efficient iterative schemes for ab initio total-energy calculations using a plane-wave basis set*, Phys. Rev. B **54**, 11169–11186 (1996).

[55] W. Setyawan and S. Curtarolo, *High-throughput electronic band structure calculations: challenges and tools*, Comp. Mat. Sci. **49**, 299–312 (2010).

[56] S. Curtarolo, W. Setyawan, S. Wang, J. Xue, K. Yang, R. H. Taylor, L. J. Nelson, G. L. W. Hart, S. Sanvito, M. Buongiorno Nardelli, N. Mingo, and O. Levy, *AFLOWLIB.ORG: A distributed materials properties repository from high-throughput ab initio calculations*, Comp. Mat. Sci. **58**, 227–235 (2012).

[57] J. P. Perdew, K. Burke, and M. Ernzerhof, *Generalized gradient approximation made simple*, Phys. Rev. Lett. **77**, 3865–3868 (1996).

[58] H. Jiang, R. I. Gomez-Abal, P. Rinke, and M. Scheffler, *First-principles modeling of localized GW LDA+U approach*, Phys. Rev. B **82**, 045108 (2010).

[59] S. C. Abrahams and J. L. Bernstein, *Rutile: Normal Probability Plot Analysis and Accurate Measurement of Crystal Structure*, J. Chem. Phys. **55**, 3206–3211 (1971).

[60] J. Pascual, J. Camassel, and H. Mathieu, *Fine structure in the intrinsic absorption edge of TiO_2*, Phys. Rev. B **18**, 5606–5614 (1978).

[61] C. Persson and A. Ferreira da Silva, *Strong polaronic effects on rutile TiO_2 electronic band edges*, Appl. Phys. Lett. **86**, 231912 (2005).

[62] N. A. Deskins and M. Dupuis, *Electron transport via polaron hopping in bulk TiO_2: A density functional theory characterization*, Phys. Rev. B **75**, 195212 (2007).

[63] S.-G. Park, B. Magyari-Köpe, and Y. Nishi, *Electronic correlation effects in reduced rutile TiO_2 within the $LDA+U$ method*, Phys. Rev. B **82**, 115109 (2010).

[64] P.-O. Löwdin, *On the Nonorthogonality Problem*, J. Adv. Quantum Chem. **5**, 185–199 (1970).

[65] L. Grunes, R. Leapman, C. Wilker, R. Hoffmann, and A. Kunz, *Oxygen K near-edge fine structure: An electron-energy-loss investigation with comparisons to new theory for selected 3d Transition-metal oxides*, Phys. Rev. B **25**, 7157–7173 (1982).

[66] J. Woicik, E. Nelson, L. Kronik, M. Jain, J. Chelikowsky, D. Heskett, L. Berman, and G. Herman, *Hybridization and Bond-Orbital Components in Site-Specific X-Ray Photoelectron Spectra of Rutile TiO_2*, Phys. Rev. Lett. **89**, 077401 (2002).

[67] C. J. Ballhausen and H. B. Gray, *Molecular orbital theory; an introductory lecture note and reprint volume* (New York, W.A. Benjamin, 1964).

[68] W. Kang and M. S. Hybertsen, *Quasiparticle and optical properties of rutile and anatase TiO_2*, Phys. Rev. B **82**, 085203 (2010).

[69] S. P. Kowalczyk, F. R. McFeely, L. Ley, V. T. Gritsyna, and D. A. Shirley, *The electronic structure of $SrTiO_3$ and some simple related oxides (MgO, Al_2O_3, SrO, TiO_2)*, Solid State Commun. **23**, 161–169 (1977).

[70] A. Malashevich, M. Jain, and S. G. Louie, *First-principles DFT GW study of oxygen vacancies in rutile TiO_2*, Phys. Rev. B **89**, 075205 (2014).

[71] H.-Y. Lee, S. J. Clark, and J. Robertson, *First-principles study of Oxygen deficiency in rutile Titanium Dioxide*, MRS Proceedings **1352** (2011).

[72] R. Gillen and J. Robertson, *Accurate screened exchange band structures for the transition metal monoxides MnO, FeO, CoO and NiO*, J. Phys.: Conden. Matt. **25**, 165502 (2013).

[73] T. Akiyama, A. J. Freeman, K. Nakamura, and T. Ito, *Electronic structures and optical properties of GaN and ZnO nanowires from first principles*, Journal of Physics: Conference Series **100**, 052056 (2008).

[74] S. J. Clark and J. Robertson, *Screened exchange density functional applied to solids*, Phys. Rev. B **82**, 085208 (2010).

[75] H. Nakai, J. Heyd, and G. E. Scuseria, *Periodic-Boundary-Condition Calculation using Heyd-Scuseria-Ernzerhof Screened Coulomb Hybrid Functional: Electronic Structure of Anatase and Rutile TiO_2*, Journal of Computer Chemistry, Japan **5**, 7–18 (2006).

[76] C. Rödl, F. Fuchs, J. Furthmüller, and F. Bechstedt,

Quasiparticle band structures of the antiferromagnetic transition-metal oxides MnO, FeO, CoO, and NiO, Phys. Rev. B **79**, 235114 (2009).

[77] F. Fuchs, J. Furthmüller, F. Bechstedt, M. Shishkin, and G. Kresse, *Quasiparticle band structure based on a generalized Kohn-Sham scheme*, Phys. Rev. B **76**, 115109 (2007).

[78] C. E. Patrick and F. Giustino, *GW quasiparticle bandgaps of anatase TiO_2 starting from DFT+U*, J. Phys.: Conden. Matt. **24**, 202201 (2012).

[79] M. Shishkin and G. Kresse, *Self-consistent GW calculations for semiconductors and insulators*, Phys. Rev. B **75**, 235102 (2007).

[80] M. Landmann, E. Rauls, and W. G. Schmidt, *The electronic structure and optical response of rutile, anatase and brookite TiO_2*, J. Phys.: Conden. Matt. **24**, 195503 (2012).

[81] S. V. Faleev, M. van Schilfgaarde, and T. Kotani, *All-Electron Self-Consistent GW Approximation: Application to Si, MnO, and NiO*, Phys. Rev. Lett. **93**, 126406 (2004).

[82] L. Y. Lim, S. Lany, Y. J. Chang, E. Rotenberg, A. Zunger, and M. F. Toney, *Angle-resolved photoemission and quasiparticle calculation of ZnO: The need for d band shift in oxide semiconductors*, Phys. Rev. B **86**, 235113 (2012).

[83] E. Z. Kurmaev, R. G. Wilks, A. Moewes, L. D. Finkelstein, S. N. Shamin, and J. Kuneš, *Oxygen x-ray emission and absorption spectra as a probe of the electronic structure of strongly correlated oxides*, Phys. Rev. B **77**, 165127 (2008).

[84] C. L. Dong, C. Persson, L. Vayssieres, A. Augustsson, T. Schmitt, M. Mattesini, R. Ahuja, C. L. Chang, and J.-H. Guo, *Electronic structure of nanostructured ZnO from x-ray absorption and emission spectroscopy and the local density approximation*, Phys. Rev. B **70**, 195325 (2004).

[85] Y. Tezuka, S. Shin, T. Ishii, T. Ejima, S. Suzuki, and S. Sato, *Photoemission and Bremsstrahlung Isochromat Spectroscopy Studies of TiO_2 (Rutile) and $SrTiO_3$*, Journal of the Physical Society of Japan **63**, 347–357 (1994).

[86] J. van Elp, R. H. Potze, H. Eskes, R. Berger, and G. A. Sawatzky, *Electronic structure of MnO*, Phys. Rev. B **44**, 1530–1537 (1991).

[87] G. A. Sawatzky and J. W. Allen, *Magnitude and Origin of the Band Gap in NiO*, Phys. Rev. Lett. **53**, 2339–2342 (1984).

[88] I. A. Drabkin, L. T. Emel'yanova, R. N. Iskenderov, and Y. M. Ksendzov, Fizika Tverdogo Tela **10**, 3082 (1968).

[89] Y. M. Ksendzov and I. A. Drabkin, Fizika Tverdogo Tela **7**, 1884 (1965).

[90] R. N. Iskenderov, I. A. Drabkin, L. T. Emel'yanova, and Y. M. Ksendzov, Fizika Tverdogo Tela **10**, 2573 (1968).

[91] A. Mang, K. Reimann, and S. Rübenacke, *Band gaps, crystal-field splitting, spin-orbit coupling, and exciton binding energies in ZnO under hydrostatic pressure*, Solid State Commun. **94**, 251–254 (1995).

[92] R. J. Powell and W. E. Spicer, *Optical Properties of NiO and CoO*, Phys. Rev. B **2**, 2182–2193 (1970).

[93] T. D. Kang, H. S. Lee, and H. Lee, *Optical Properties of Black NiO and CoO Single Crystals Studied with Spectroscopic Ellipsometry*, Journal of the Korean Physical Society **50**, 632–637 (2007).

[94] D. C. Reynolds, D. C. Look, B. Jogai, C. W. Litton, G. Cantwell, and W. C. Harsch, *Valence-band ordering in ZnO*, Phys. Rev. B **60**, 2340–2344 (1999).

[95] A. K. Cheetham and D. A. O. Hope, *Magnetic ordering and exchange effects in the antiferromagnetic solid solutions MnNiO*, Phys. Rev. B **27**, 6964–6967 (1983).

[96] A. Floris, S. de Gironcoli, E. K. U. Gross, and M. Cococcioni, *Vibrational properties of MnO and NiO from DFT+U-based density functional perturbation theory*, Phys. Rev. B **84**, 161102 (2011).

[97] B.-C. Shih, T. A. Abtew, X. Yuan, W. Zhang, and P. Zhang, *Screened Coulomb interactions of localized electrons in transition metals and transition-metal oxides*, Phys. Rev. B **86**, 165124 (2012).

[98] V. I. Anisimov, M. A. Korotin, and E. Z. Kurmaev, *Band-structure description of Mott insulators (NiO, MnO, FeO, CoO)*, J. Phys.: Conden. Matt. **2**, 3973 (1990).

[99] L. Wang, T. Maxisch, and G. Ceder, *Oxidation energies of transition metal oxides within the GGA+U framework*, Phys. Rev. B **73**, 195107 (2006).

[100] C. Franchini, R. Podloucky, J. Paier, M. Marsman, and G. Kresse, *Ground-state properties of multivalent manganese oxides: Density functional and hybrid density functional calculations*, Phys. Rev. B **75**, 195128 (2007).

[101] S. Kobayashi, Y. Nohara, S. Yamamoto, and T. Fujiwara, *GW approximation with LDA+U method and applications to NiO, MnO, and V_2O_3*, Phys. Rev. B **78**, 155112 (2008).

[102] B. E. F. Fender, A. J. Jacobson, and F. A. Wedgwood, *Covalency Parameters in MnO, α-MnS, and NiO*, J. Chem. Phys. **48**, 990–994 (1968).

[103] R. Sakuma and F. Aryasetiawan, *First-principles calculations of dynamical screened interactions for the transition metal oxides MO (M=Mn, Fe, Co, Ni)*, Phys. Rev. B **87**, 165118 (2013).

[104] N. Alidoust, M. C. Toroker, and E. A. Carter, *Revisiting photoemission and inverse photoemission spectra of nickel oxide from first principles: implications for solar energy conversion*, J. Phys. Chem. B **28**, 7963–7971 (2014).

[105] J.-L. Li, G.-M. Rignanese, and S. G. Louie, *Quasiparticle energy bands of NiO in the GW approximation*, Phys. Rev. B **71**, 193102 (2005).

[106] V. I. Anisimov, J. Zaanen, and O. K. Andersen, *Band theory and Mott insulators: Hubbard U instead of Stoner I*, Phys. Rev. B **44**, 943–954 (1991).

[107] A. Fujimori and F. Minami, *Valence-band photoemission and optical absorption in nickel compounds*, Phys. Rev. B **30**, 957–971 (1984).

[108] S. Massidda, A. Continenza, M. Posternak, and A. Baldereschi, *Quasiparticle energy bands of transition-metal oxides within a model GW scheme*, Phys. Rev. B **55**, 13494–13502 (1997).

[109] R. Zimmermann, P. Steiner, R. Claessen, F. Reinert, S. Hüfner, P. Blaha, and P. Dufek, *Electronic structure of 3d-transition-metal oxides: on-site Coulomb repulsion versus covalency*, J. Phys.: Conden. Matt. **11**, 1657 (1999).

[110] W. L. Roth, *Magnetic Structures of MnO, FeO, CoO, and NiO*, Phys. Rev. **110**, 1333–1341 (1958).

[111] R. H. Taylor, F. Rose, C. Toher, O. Levy, K. Yang, M. Buongiorno Nardelli, and S. Curtarolo, *A RESTful API for exchanging Materials Data in the AFLOWLIB.org consortium*, Comp. Mat. Sci. **93**, 178–192 (2014).

[112] A. Calzolari, A. Ruini, and A. Catellani, *Anchor Group versus Conjugation: Toward the Gap-State Engineering*

of Functionalized ZnO(10$\bar{1}$0) Surface for Optoelectronic Applications, J. Am. Chem. Soc. **133**, 5893–5899 (2011).

[113] X. Ma, Y. Wu, Y. Lv, and Y. Zhu, *Correlation Effects on Lattice Relaxation and Electronic Structure of ZnO within the GGA+U Formalism*, J. Phys. Chem. C **117**, 26029–26039 (2013).

[114] J. E. Jaffe and A. Zunger, *Theory of the band-gap anomaly in ABC_2 chalcopyrite semiconductors*, Phys. Rev. B **29**, 1882–1906 (1984).

[115] R. A. Powell, W. E. Spicer, and J. C. McMenamin, *Photoemission Studies of Wurtzite Zinc Oxide*, Phys. Rev. B **6**, 3056–3065 (1972).

[116] L. Ley, R. A. Pollak, F. R. McFeely, S. P. Kowalczyk, and D. A. D. A. Shirley, *Total valence-band densities of states of III-V and II-VI compounds from x-ray photoemission spectroscopy*, Phys. Rev. B **9**, 600–621 (1974).

[117] C. J. Vesely and D. W. Langer, *Electronic Core Levels of the IIB-VIA Compounds*, Phys. Rev. B **4**, 451–462 (1971).

[118] D. Vogel, P. Krüger, and J. Pollmann, *Self-interaction and relaxation-corrected pseudopotentials for II-VI semiconductors*, Phys. Rev. B **54**, 5495–5511 (1996).

[119] S. j. Hu, S. s. Yan, M. w. Zhao, and L. m. Mei, *First-principles LDA+U calculations of the Co-doped ZnO magnetic semiconductor*, Phys. Rev. B **73**, 245205 (2006).

[120] T. R. Paudel and W. R. L. Lambrecht, *First-principles calculation of the O vacancy in ZnO: A self-consistent gap-corrected approach*, Phys. Rev. B **77**, 205202 (2008).

[121] P. Gopal, L. Agapito, L. Liyanage, S. Curtarolo, M. Fornari, and M. Buongiorno Nardelli, , in preparation (2014).

[122] R. J. Mathar, *Mutual conversion of three flavors of Gaussian type orbitals*, Int. J. Quantum. Chem. **90**, 227–243 (2002).

[123] Pseudopotentials and PAOs used in this work are publicly available at `http://qe-forge.org/gf/project/pslibrary/`.

[124] W. J. Hehre, R. F. Stewart, and J. A. Pople, *Self-Consistent Molecular-Orbital Methods. I. Use of Gaussian Expansions of Slater-Type Atomic Orbitals*, J. Chem. Phys. **51**, 2657–2664 (1969).

[125] J. B. Collins, P. von R. Schleyer, J. S. Binkley, and J. A. Pople, *Self-consistent molecular orbital methods. XVII. Geometries and binding energies of second-row molecules. A comparison of three basis sets*, J. Chem. Phys. **64**, 5142–5151 (1976).

[126] D. Feller, *The role of databases in support of computational chemistry calculations*, J. Comp. Chem. **17**, 1571–1586 (1996).

[127] R. J. Mathar, *Orthogonal Linear Combinations of Gaussian Type Orbitals* (2009).

[128] A. F. Izmaylov, G. E. Scuseria, and M. J. Frisch, *Efficient evaluation of short-range Hartree-Fock exchange in large molecules and periodic systems*, J. Chem. Phys. **125**, 104103 (2006).